PHYSICAL REVIEW B VOLUME 61, NUMBER 4 15 JANUARY 2000-II

Linear and nonlinear optical properties of group-III nitrides

V. I. Gavrilenko* and R. Q. Wu
Department of Physics and Astronomy, California State University, Northridge, California 91330

(Received 16 February 1999; revised manuscript received 4 October 1999)

Linear and nonlinear [second harmonic generation (SHG)] optical functions of cubic and hexagonal BN, AlN, GaN, and InN have been studied by using the first-principles full-potential linearized augmented plane-wave method. Equilibrium lattice constants are determined from the total-energy minimization method. The calculated spectra of the second-order optical susceptibility show pronounced structures related to the two-photon resonances. In materials with heavy metals there are remarkable contributions from the single-photon transitions. Line shapes of the linear and particularly the nonlinear optical spectra of GaN and InN crystals are very sensitive to the interactions between the conduction bands and metallic *d* states. Studies of the nonlinear optical susceptibilities in both wurtzite and cubic crystals show high sensitivity of the SHG spectra to the changes of atomic structure.

I. INTRODUCTION

Group-III nitrides are promising materials for various technological applications, such as short-wavelength light-emitting diodes, semiconductor lasers, and optical detectors.[1] Electron band-structure parameters and optical properties of group-III nitrides including their linear[2–15] and nonlinear optical response functions[16–20] have been extensively studied in the last decade both theoretically and experimentally.

Nonlinear optical properties such as the second harmonic generation (SHG) and the sum frequency generation (SFG) spectroscopies have a great potential to be used as novel efficient techniques for material characterization. The optical second-order susceptibility functions ($\chi^{(2)}$) are known to be very sensitive to the changes of symmetry.[21] This makes SHG and SFG spectroscopies extremely promising for surface studies,[22] especially for monitoring surface contaminations and surface chemical reactions (see Ref. 23 and references therein). Owing to technical difficulties and computational demands, however, the nonlinear optical spectra of the group-III nitrides are rarely studied using the first-principles electronic structure theories and are still poorly understood.

In this paper we report results of a systematic study of electronic structure and linear, and nonlinear optical properties of InN, GaN, AlN, and BN crystals in the zinc-blende and wurtzite structures. We used the first-principles full-potential linearized augmented plane-wave (FLAPW) method. The equilibrium lattice constants are determined from the total-energy minimization method. To understand the nature of optical transitions and other relevant effects on the calculated optical functions, we study the local densities of states (LDOS's) and other electronic properties of these materials.

This work is based on a single-electron picture, namely, we neglected the excitonic effects and the local-field corrections. As shown previously, these effects in the bulk materials might change values of the predicted linear and nonlinear optical spectra by 20–30 %, especially in the spectral regions of direct gaps in semiconductors.[18,24–26]

II. METHOD

The electronic band structure and the optical function computations are based on the FLAPW theory.[27,28] In the FLAPW method no shape approximation is made for charge density, potential, and matrix elements.[27] FLAPW calculations have provided very accurate results of linear and nonlinear optical functions for many cubic $A^{\mathrm{III}}B^{\mathrm{V}}$ compound semiconductors as well as of wurtzite AlN and GaN crystals (see Ref. 29 and references therein).

A. Electron band structure

To take into account the exchange and correlation effects, we used formulas of both local density approximation (LDA, with the von Barth–Hedin formula[31]) and the generalized gradient approximation (GGA) (with the Perdew-Bucky formula).[32] The FLAPW-GGA approach has been successfully applied for the determination of electronic and optical properties of various materials.[33] The core states are treated fully relativistically, while the spin-orbit coupling interactions among the valence states are treated second-variationally.[28] Energy cutoffs of 15 and 100 Ry are employed to describe the augmented plane-wave basis functions and the star functions for the charge density and potential in the interstitial region, respectively. We found that BN and AlN require less **k** points than GaN and InN. 2500 **k** points in the full Brillouin zone (BZ) are employed to obtain reliable results.

B. Optical functions

The linear ($\chi^{(1)}$) and nonlinear ($\chi^{(2)}$) optical susceptibilities are computed through the optical response theory for complex resonance functions.[34] This approach requires less **k** points, but it is slower then other often-used methods with δ functions to determine the imaginary part of $\chi^{(1)}$ and $\chi^{(2)}$ with subsequent evaluations for the real parts from the Kramers-Krönig relationship.[19,35]

Here the optical functions $\chi^{(1)}$ and $\chi^{(2)}$ were calculated within random-phase approximation by neglecting the non-

0163-1829/2000/61(4)/2632(11)/$15.00

TABLE I. The measured (at $T=300$ K) and calculated (at $T=0$ K) lattice constants (in Å) of zinc-blende and wurtzite nitrides. Experimental data are given in parentheses.

	BN	AlN	GaN	InN
		Zinc blende		
This work	3.619 (3.615[a])	4.42 (4.38[b])	4.55 (4.5[c])	5.02 (4.98[d])
Ref. 5		4.342	4.460	4.932
Ref. 2	3.619	4.357	4.433	4.922
		Wurtzite		
a	2.56 (2.55)[e]	3.13 (3.11)[f]	3.24 (3.19)[f]	3.59 (3.54)[g]
c	4.22 (4.23)[e]	5.09 (4.98)[f]	5.24 (5.20)[f]	5.81 (5.69)[g]
c/a	1.644 (1.656)[e]	1.618 (1.601)[f]	1.614 (1.63)[f]	1.621 (1.61)[g]

[a] Reference 46.
[b] Reference 47.
[c] Reference 48.
[d] Reference 49.
[e] Reference 50.
[f] Reference 51.
[g] Reference 52.

locality of the velocity operator.[26] The nonlinear optical susceptibility $\chi^{(2)}$ in longitudinal (length) gauge is given by[36]

$$\begin{aligned}\chi^{(2)}_{ijk}(-2\omega,\omega,\omega) &= -N\frac{e^3}{\hbar^2}\sum_{g,n,n'}\Bigg\{\frac{(r_i)_{gn}\{(r_j)_{n,n'},(r_k)_{n'g}\}}{(2\omega-\omega_{ng}+i\Gamma_{ng})(\omega-\omega_{n'g}+i\Gamma_{n'g})} \\ &\quad+\frac{\{(r_k)_{gn},(r_j)_{n'n}\}(r_i)_{ng}}{(2\omega+\omega_{ng}+i\Gamma_{ng})(\omega+\omega_{n'g}+i\Gamma_{n'g})} \\ &\quad-\frac{\{(r_j)_{ng},(r_k)_{gn'}\}(r_i)_{n'n}}{(2\omega-\omega_{nn'}+i\Gamma_{nn'})}\Bigg[\frac{1}{(\omega+\omega_{n'g}+i\Gamma_{n'g})} \\ &\quad+\frac{1}{(\omega-\omega_{ng}+i\Gamma_{ng})}\Bigg]\Bigg\}\rho^{(0)}_g, \end{aligned} \tag{1}$$

where the curly-bracket notation indicates all permutations with respect to the Cartesian coordinates, N is the number density of electrons, $\hbar\omega_{ij}$ is the energy difference, and Γ_{ij} the corresponding broadening parameter, between levels i and j. The Fermi distribution function $\rho^{(0)}_g$ was taken at zero temperature. Matrix elements $\mathbf{r}_{ng}$ were determined by $\mathbf{r}_{ng}=\mathbf{p}_{ng}/im\omega_{ng}$ through momentum matrix elements $\mathbf{p}_{ng}$. The sum in Eq. (1) covers all occupied and empty states; however, the values of the triple matrix element products are nonzero only if the electron states in resonant denominator terms [e.g., $n-g$ and $n'-g$ states in the first term of Eq. (1)] have different occupancies. This procedure accounts all transitions with virtual electron and virtual hole contributions. The calculation of the SHG by Eq. (1) using additional occupancy factors in the code is close to the method used in Ref. 29 and provides very similar results.

The LDA is well known to underestimate band gaps of semiconductors, which in turn causes some errors for the linear and higher-order optical response functions. The gradient corrections in the GGA somewhat improve the situation but cannot solve the problem completely, as is demonstrated below. For a better agreement with experiment the quasiparticle corrections[37] (QP) with inclusion of both static and dynamical interactions[24] are needed, which makes the calculation procedures extremely complex and time demanding. The many-body effects can be reasonably treated by using scissorslike corrections both to the band energies (Δ) and to the velocity matrix elements.[38] To match the experimental gap energies, we shift the conduction bands (c bands) by a value of Δ and renormalize the corresponding momentum matrix elements as[29]

$$\tilde{\mathbf{v}}_{nm}=\mathbf{v}_{nm}\frac{\omega_{nm}+(\Delta/\hbar)(\delta_{nc}-\delta_{mc})}{\omega_{nm}}. \tag{2}$$

The corrections to the momentum matrix elements, as discussed in the literature, appear to improve the results of optical spectra further from the case with corrections merely to the band energies.[20,29,39]

III. ELECTRON BAND STRUCTURE

We determined the equilibrium lattice constants a (cubic) and a and c (hexagonal) through the total-energy minimization method. In Table I we compare the calculated data with experiment and with the results obtained from previous calculations. The LDA values of lattice constants[2,5] are smaller than the experimental data (i.e., smaller lattices). This makes energy gaps larger as a result of the hydrostatic compression. By contrast, our GGA data are slightly larger (by 0.8–1.0 %) compared to the experimental lattice sizes (see Table I). This may shrink the bandwidths and gaps. It should be noted that all the calculations are performed here at zero temperature. The lattice constant is temperature dependent. The experimental values listed in Table I are obtained at room temperature. In view of the sensitivity of the electron energy structure and optical functions to the lattice constant (as well as to the other temperature-dependent effects) this should be taken into account by comparison between theoretical and experimental data.

The calculated energy gap values (E_g) are given in Table II. To avoid computational complexity, the QP corrections Δ are used in most theoretical papers as a scissorslike operator.

TABLE II. Band-structure parameters (in eV) of zinc-blende and wurtzite nitrides: values of quasiparticle corrections Δ used in present work; the calculated and measured values of the energy gap E_g; energy positions E_d of the d states with respect to the Fermi level.

	BN	AlN	GaN	InN
	Zinc blende			
Δ	0.0	0.0	0.5	1.6
E_g				
Expt.	6.1,[a] 6.2[b,d]		3.3[a]	1.9[a]
Present work (GGA)	4.6	3.30	2.4[c]	1.9[c]
Reference 10	6.1	5.2	3.8	
E_d				
Present work (GGA)			−13.9	−13.5
Reference 10			−13.6	−13.4
	Wurtzite			
Δ	0.0	1.8	0.5	1.65
E_g				
Expt.	6.1,[a] 6.2[b]	6.3	3.3[a]	1.9[a]
Present work (GGA)	4.6	3.30	2.4[c]	1.9[c]
Reference 10	6.1	5.2	3.8	
E_d				
Present work (GGA)			−13.9	−13.5
Reference 10			−13.6	−13.4

[a] Reference 46.
[b] Reference 53.
[c] With QP correction.
[d] Reference 60.

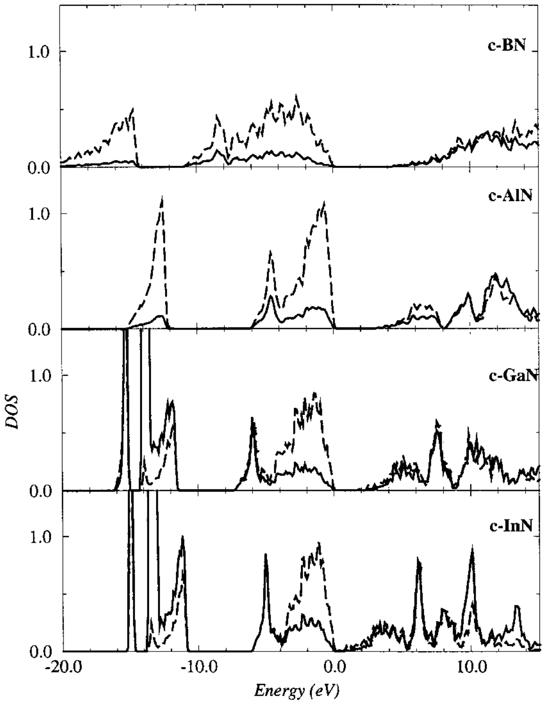

FIG. 1. The calculated local densities of states projected to the muffin-tin spheres of N (dashed line) and cation element (solid line) in the cubic group-III nitride crystals.

The value of Δ was widely chosen to match experimental E_g data. However, due to the strong $\mathbf{k}$ dependence of Δ (see, e.g., Ref. 26 and references therein) this does not improve the disagreement between calculated and measured optical functions in high-energy spectral region. In other words, the scissorslike QP corrections do not improve the bandwidth of the c band. Therefore for a better agreement with experiment, GW corrections are required.[37,40] In the absence of reliable experimental results of optical functions in high-energy regions of BN and cubic AlN, we did not use the QP corrections for these materials. The values of the QP correction Δ are determined in this work by fitting the main features of the calculated linear spectra (E_2 transitions only) to the experimental $\epsilon_2(\omega)$ curve.[3] The value of $\Delta = 0.5\,\mathrm{eV}$ in GaN obtained through this procedure is remarkably smaller than the value of $\Delta = 1.4\,\mathrm{eV}$ required to match the experimental gap. The spectral location of calculated features (particularly SHG peaks) should be closer to experimental spectra if main optical gaps are matched. The effect of this QP correction on calculated optical functions is demonstrated below for SHG spectra of cubic GaN. For InN the values of Δ are determined by fitting the calculated E_g value to the experimental one.

To understand the calculated optical susceptibility functions we studied the LDOS spectra. The calculated LDOS curves for BN, AlN, GaN, and InN are given in Figs. 1 and 2. Compared to other $A^{\mathrm{III}}B^{\mathrm{V}}$ materials, the band structures of the group-III nitrides show some important features: the d bands of metal elements in GaN and InN are located quite close to the valence sp bands. The energy position of Ga $3d$ states in both cubic and hexagonal GaN is at -13.9 eV, a result that agrees well with that obtained in the previous linearized muffin-tin orbital (LMTO) calculation,[4] -13.3 eV, but is still remarkably higher than the energy position of the Ga $3d$ peak in an x-ray photoemission experiment, $-17.1 \pm 0.1\,\mathrm{eV}$.[4] In all the compounds studied here the valence bands are dominated by the $2p$ bonding states of nitrogen at

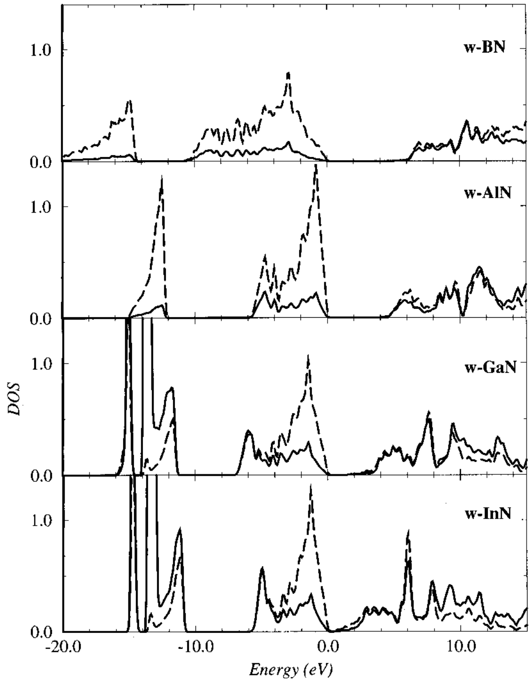

FIG. 2. The same as Fig. 1 but for hexagonal group-III nitride crystals.

TABLE III. Macroscopic dielectric constants of zinc-blende and wurtzite group-III nitride crystals.

	BN	AlN	GaN	InN
Present work (cubic)	4.51	4.61	5.71	7.46
Reference 2	4.14	3.86	4.68	7.16
Reference 16	4.56	4.61	5.74	
Reference 14	4.54	4.46		
Expt.	4.41[a]	4.68[b]	5.7,[c] 5.46[d]	8.4[e]
	$\epsilon_\perp$			
Present work (hex.)	4.50	4.05	5.87	7.37
Reference 2	4.19	3.91	4.71	7.27
Reference 16	4.51	4.42	5.54	
Reference 14	4.50	4.38		
Reference 15			5.21	
	$\epsilon_\parallel$			
Present work (hex.)	4.61	4.19	5.89	7.25
Reference 2	4.14	3.77	4.62	6.94
Reference 16	4.56	4.70	5.60	
Reference 14	4.67	4.61		
Reference 15			5.41	
	ϵ_∞			
Present work (hex.)	4.53	4.10	5.88	7.33
Reference 2	4.14	3.86	4.68	7.16
Reference 16	4.56	4.61	5.74	
Reference 14	4.56	4.46		
Reference 15			5.28	
Expt.	4.50[f]	4.68[b]	5.35±0.2[g]	8.4[e]

[a] The value of $\epsilon_0 = n_0^2$ is obtained from the refractive index $n_0 = 2.1$ measured in Ref. 54.

[b] Reference 55.

[c] Reference 56.

[d] The value of $\epsilon_0 = n_0^2$ is obtained from refractive index $n_0 = 2.34$ measured in Ref. 53.

[e] Reference 57.

[f] Reference 46.

[g] Reference 58.

the top of the valence band. In the absence of the metal d states, the LDOS's of N $2s$ bonding states in AlN and BN are much higher than those of the electronic states of metal[60] (see Figs. 1 and 2). The electronic transitions from the N $2s$ band make remarkable contributions to the second-order optical susceptibility due to the double-frequency resonances as discussed below.

IV. OPTICAL FUNCTIONS

A. Static dielectric constants

The calculated values of the static macroscopic dielectric constants ϵ_0 are given in Table III, in comparison with the data in the literature. We can state quite good agreement of our data with the previously published results. Comparison of our results with previous LMTO–atomic sphere approximation (ASA) data[2] presented in Table III shows that LMTO data systematically underestimate experimental and FLAPW results. The LMTO-ASA values of static ϵ_0 deviate more significantly from the results of our full-potential and other pseudopotential calculations (see Table III). By approximative treatment of the potential in the interstitial regions (as by the ASA method[30] used in Ref. 2), the choice of the atomic sphere radius affects somewhat the amplitudes of the calculated optical functions. Therefore the deviations observed could be considered as measures for the errors in optical functions caused by approximative versus precise description of the potential energy in nitrides.

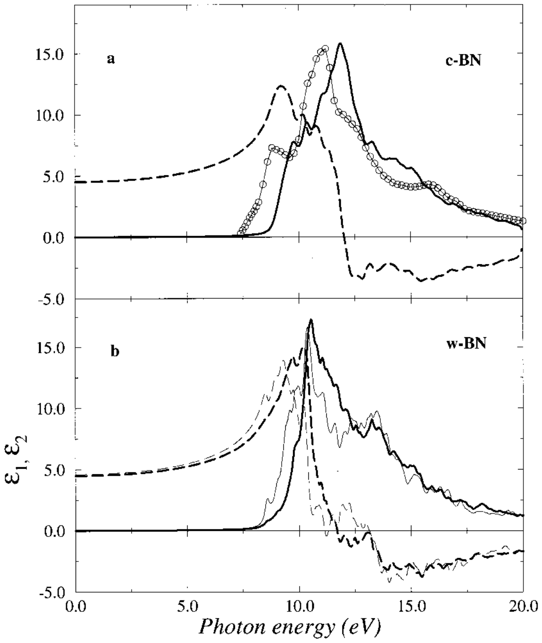

FIG. 3. The calculated spectra of real (dashed lines) and imaginary parts (solid lines) of the linear dielectric function $\epsilon(\omega)$ of the (a) cubic and (b) hexagonal BN crystals. In panel (b) values of $\epsilon_\parallel$ and of $\epsilon_\perp$ are shown by bold and thin lines, respectively. In panel (a) experimental data of Ref. 41 are presented by circles.

In hexagonal crystals the anisotropy of static ϵ is not strong but is noticeable in all the materials studied here. Our data clearly indicate the tendency of changing signs of uniaxial anisotropy degree $[\delta\epsilon = 3(\epsilon_\parallel - \epsilon_\perp)/\epsilon_\parallel + 2\epsilon_\perp]$ when the cations change from simple to heavy metals: $\delta\epsilon > 0$ for BN and AlN, $\delta\epsilon \simeq 0$ for GaN, but $\delta\epsilon < 0$ for InN (see Table III). Small positive values of $\delta\epsilon$ for BN and AlN are also reported in Refs. 14 and 18 as obtained from pseudopotential calculations. Our value of $\delta\epsilon \simeq 0$ for GaN is close to that obtained in Ref. 18.

B. Linear optical functions

The calculated dielectric functions $\epsilon(\omega)$ are presented in Figs. 3–6. The calculated $\epsilon(\omega)$ spectra of BN and AlN (Figs. 3 and 4) are in good agreement with LMTO-ASA results.[2] However, for BN, our theoretical spectra as well as LMTO-ASA results[2] are shifted to the higher-energy region compared to the experimental result of Im[$\epsilon(\omega)$] obtained from the Kramers-Krönig analysis of reflectance measurements.[41] The LMTO values of the imaginary part of ϵ of BN are only slightly lower than the FLAPW data (Fig. 3).

In Fig. 5, the results for GaN obtained in this work are given together with the experimental data of spectroellipsometry measurements.[3] An overall good agreement with ex-

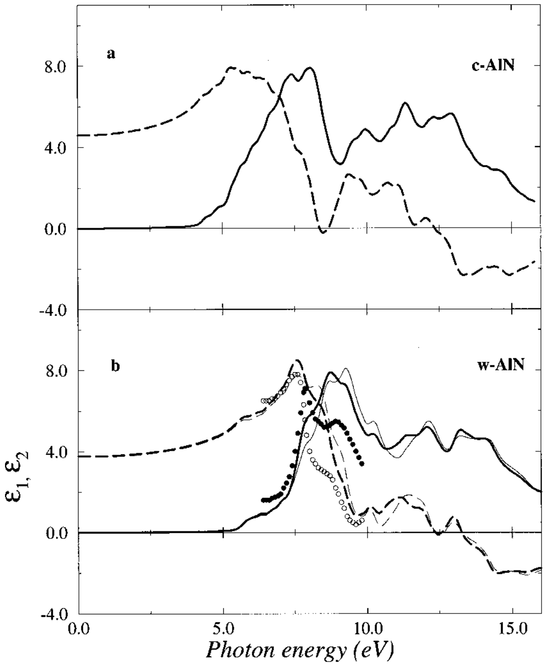

FIG. 4. The calculated spectra of real (dashed lines) and imaginary parts (solid lines) of the linear dielectric function $\epsilon(\omega)$ of the (a) cubic and (b) hexagonal AlN crystals. In panel (b) values of $\epsilon_\parallel$ and of $\epsilon_\perp$ are shown by bold and thin lines, respectively. Experimental data (Ref. 59) are presented by open (ϵ_1) and filled (ϵ_2) circles.

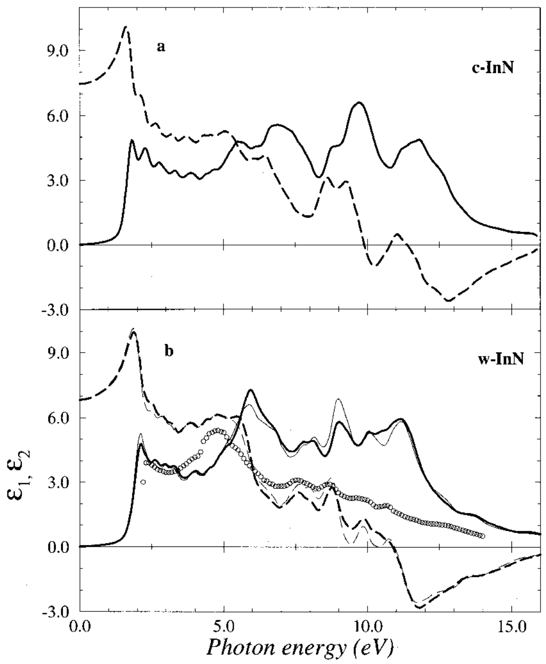

FIG. 6. The calculated spectra of real (dashed lines) and imaginary parts (solid lines) of the linear dielectric function $\epsilon(\omega)$ of the (a) cubic and (b) hexagonal InN crystals. In panel (b) values of $\epsilon_\parallel$ and of $\epsilon_\perp$ are shown by bold and thin lines, respectively. Experimental results of ϵ_2 (Ref. 42) are shown by open circles.

periment is achieved for both real and imaginary parts of $\epsilon(\omega)$. This demonstrates the accuracy and reliability of our FLAPW approach for predicting optical spectra.

Spectra of $\epsilon(\omega)$ of InN (Fig. 6) are calculated in this work with QP corrections of $\Delta = 1.6$ eV (cubic) and $\Delta = 1.65$ eV (hexagonal; see Table II). The line shapes of our FLAPW spectra are in reasonable agreement with previous LMTO-ASA results.[2] In the region near the threshold, however, the intensities of our FLAPW ϵ_2 spectra are remarkably higher than that of the LMTO-ASA calculations[2] for both cubic and hexagonal crystals. In wurtzite InN crystals the experimental values[42] of ϵ_2 in the low-energy region are about a factor of 1.5 higher in magnitude than the results predicted by LMTO-ASA calculations. The line shape of our FLAPW spectra is in good agreement with experiment [see Fig. 6(b)]. It appears that ϵ_2 of InN is sensitive to the accuracy of wave functions and eigenvalues. The experimental verification of $\epsilon(\omega)$ of InN is highly desirable.

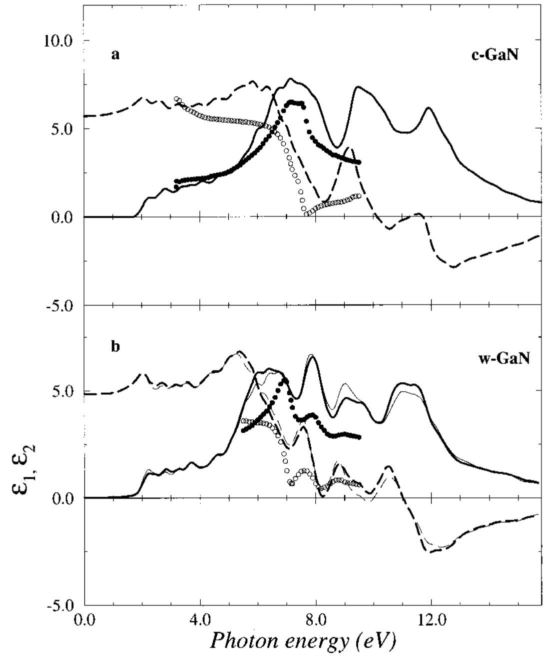

FIG. 5. The calculated spectra of real (dashed line) and imaginary parts (solid line) of the linear dielectric function $\epsilon(\omega)$ of the cubic GaN crystal. Experimental data obtained by the spectroellipsometry (Ref. 3) are shown by open (ϵ_1) and filled (ϵ_2) circles.

C. Second-order optical susceptibilities

In Table IV we listed values of the static second-order optical susceptibility constants, d (cubic) and d_{xzx} and d_{zzz} (hexagonal). In cubic materials our FLAPW+GGA+Δ data are quite close to those obtained from the LMTO+LDA+QP calculations,[20] and in hexagonal crystals our results are quite close (with somewhat enhanced absolute values) to those obtained from the previous FLAPW+LDA+QP calculations of AlN and GaN.[19] Pseudopotential theory based on LDA+QP (Ref. 16) predicted smaller values of d, d_{xzx}, and d_{zzz} for AlN and GaN, which are further reduced if the local-field effects are taken into account.[18]

The frequency dependences of the nonvanishing components (*xyz* in cubic crystals and *xzx*, *zxx*, and *zzz* in hexagonal crystals) of the $\chi^{(2)}$ function are given in Figs. 7–18. In contrast to the linear optical functions, the calculated spectra of $\chi^{(2)}_{ijk}(-2\omega,\omega,\omega)$ show pronounced structures contributed

TABLE IV. The calculated values of static second-order optical susceptibility, for zinc-blende (d) and wurtzite (d_{xzx}, d_{zzz}) group-III nitrides (in pm/V).

	BN	AlN	GaN	InN
		d		
This work	1.04	−1.0	11.7	8.93
Reference 20	2.4	−0.4, −0.23	10.6	
Reference 18	1.7	0.005	5.0	
		d_{xzx}		
This work	−1.25	−0.35	−5.86	5.62
Reference 19		−0.25	−4.27	
Reference 18	−0.9	−0.1	−2.1	
		d_{zzz}		
This work	1.61	−4.21	10.42	6.17
Reference 19		−3.77	6.03	
Reference 18	1.7	−2.3	3.5	

from both single- and double-frequency resonant terms. To analyze these contributions to the SHG spectra, it is helpful to compare $\chi^{(2)}$ and the linear optical ϵ_2 spectra.[43] To this end, the values of ϵ_2 are shown in the bottom panels as functions of both $\omega/2$ and ω. One can clearly see that the main contributions to the $\chi^{(2)}$ spectra come from two-photon resonances [cf. $\epsilon_2(\omega/2)$]. The single-photon resonances [cf. $\epsilon_2(\omega)$] contribute mainly to the high-frequency parts with much smaller amplitudes. The LDOS curves in Figs. 1 and 2 show that the valence bands of all group-III nitrides are dominated by the nitrogen $2p$ states. These electronic states as well as the states close to the bottom of the conduction bands provide the main contributions to the predicted SHG spectra of group-III nitrides. In the high-energy regions there are some features that arise from the double-frequency resonances from the N $2s$ states (e.g., the structure at 10.0 eV for BN in Fig. 7). Comparisons between the calculated spectra of $\chi^{(2)}$ for different nitrides indicate a clear trend that the

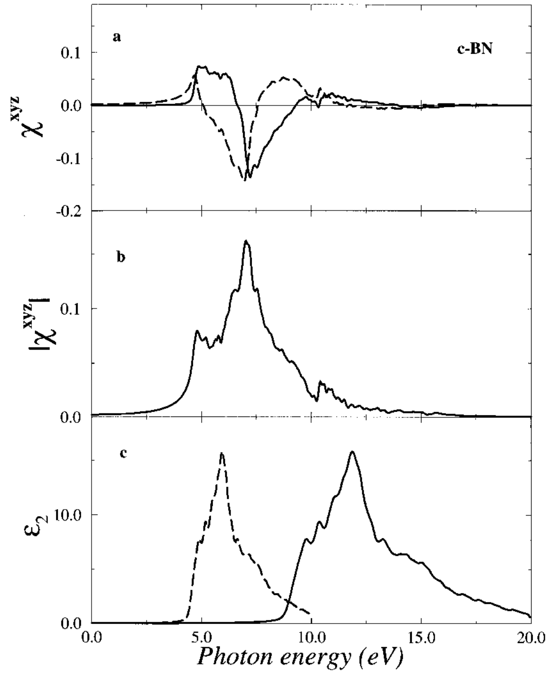

FIG. 7. The calculated spectra of the (a) real (dashed line) and imaginary parts (solid line) and (b) absolute values of the second-order optical susceptibility function $\chi^{(2)}_{xyz}(-2\omega,\omega,\omega)$ of the cubic BN crystal. In the panel (c) the spectra of $\epsilon_2(\omega/2)$ (dashed line) and $\epsilon_2(\omega)$ (solid line) are shown.

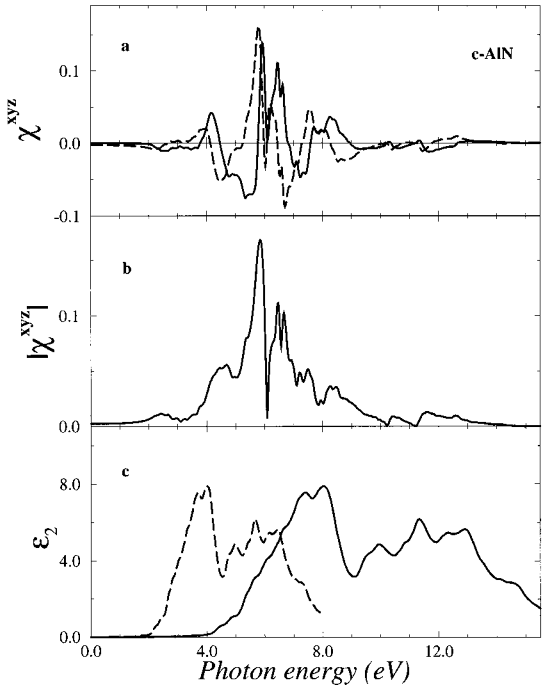

FIG. 8. The same as Fig. 7 but for a cubic AlN crystal.

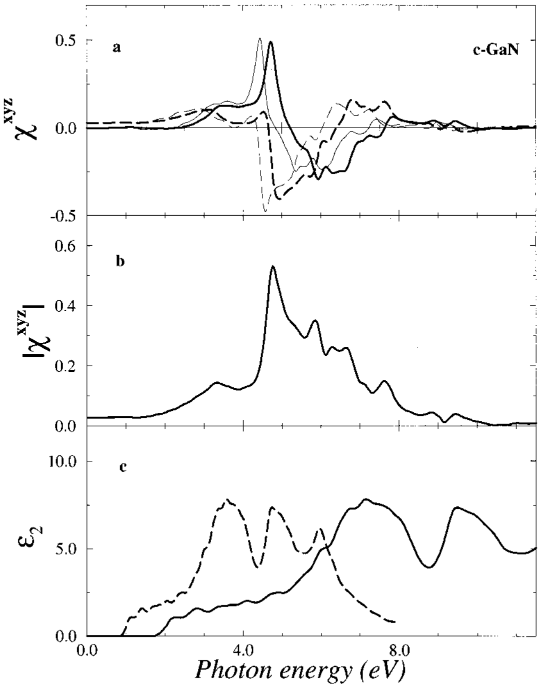

FIG. 9. The same as Fig. 7 but for a cubic GaN crystal. In the panel (a) corresponding functions calculated without the QP correction are shown.

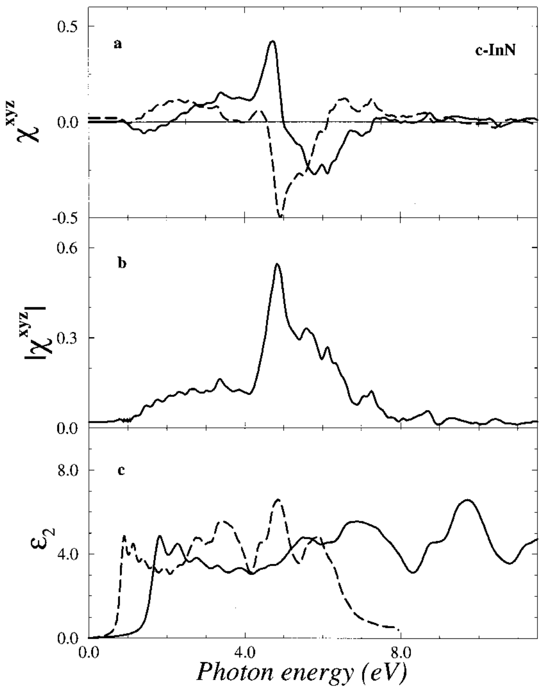

FIG. 10. The same as Fig. 7 but for a cubic InN crystal.

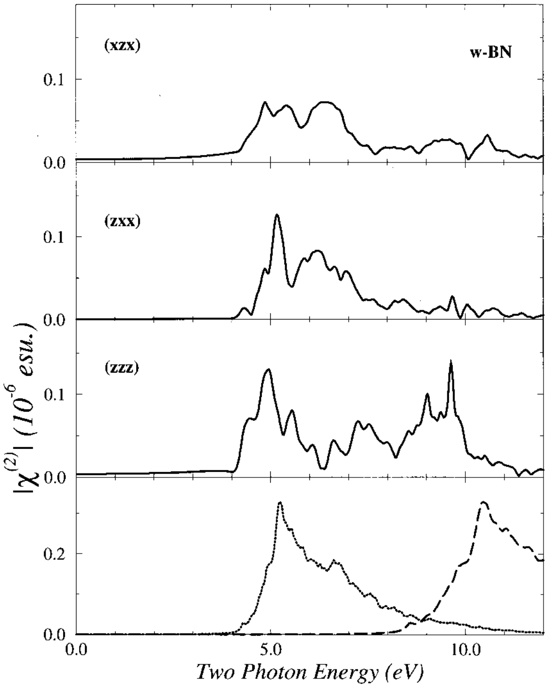

FIG. 12. The calculated absolute value spectra $|\chi^{(2)}_{ijk}|$ of the wurtzite BN crystal. In the bottom panel the spectra of $\epsilon_2(\omega/2)$ (dashed line) and $\epsilon_2(\omega)$ (dotted line) are shown with scaled amplitudes.

single-frequency resonance contributions to SHG are enhanced in compounds with heavier metals (cf. Figs. 9, 10, and 15–18). For BN, for example, only small contributions from the single-frequency resonances to the $\chi^{(2)}$ spectra can be found in the high-energy region (see Figs. 7 and 12). By contrast, the single-frequency resonance terms contribute almost in the whole spectral range for GaN and InN (cf. Figs. 9, 10, 16, and 18). The effect of QP corrections to SHG spectra is demonstrated for cubic GaN in Fig. 9. We believe that due to the reasons discussed above, the value of

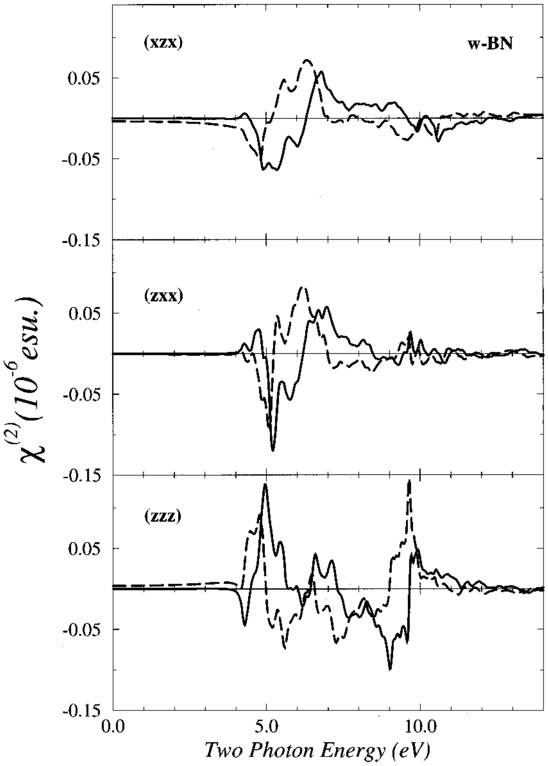

FIG. 11. The calculated spectra of the second-order optical susceptibility components $\chi^{(2)}_{ijk}(-2\omega,\omega,\omega)$ of the wurtzite BN crystal. The real and imaginary parts are shown by dashed and solid lines, respectively.

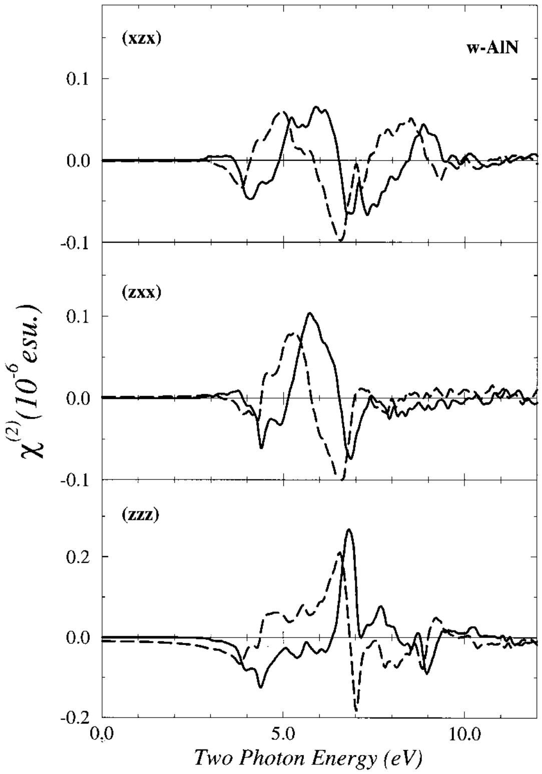

FIG. 13. The same as Fig. 11 but for a wurtzite AlN crystal.

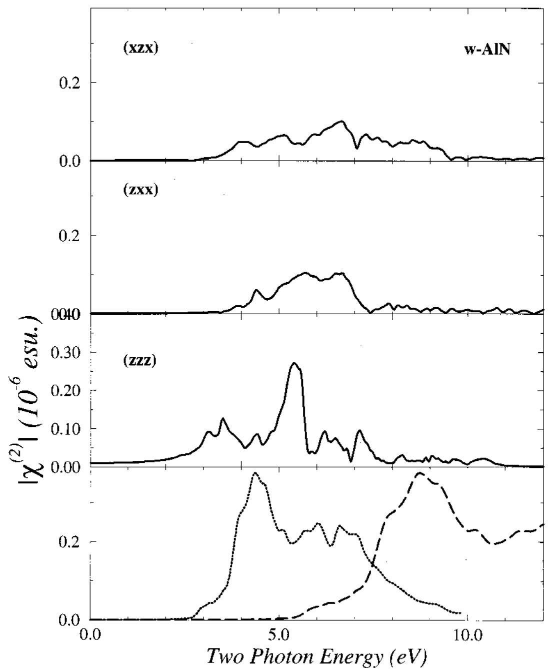

FIG. 14. The same as Fig. 12 but for a wurtzite AlN crystal.

$\Delta = 0.5$ eV, needed to match the experimental E_2 energy in GaN, is more reasonable for the spectral location predictions of the most prominent SHG resonances in GaN. For hexagonal AlN the calculated SHG spectra (Figs. 13 and 14) agree well with the previous FLAPW-LDA results,[19] indicating that the gradient corrections are less important for the line shape of optical functions in nitrides.

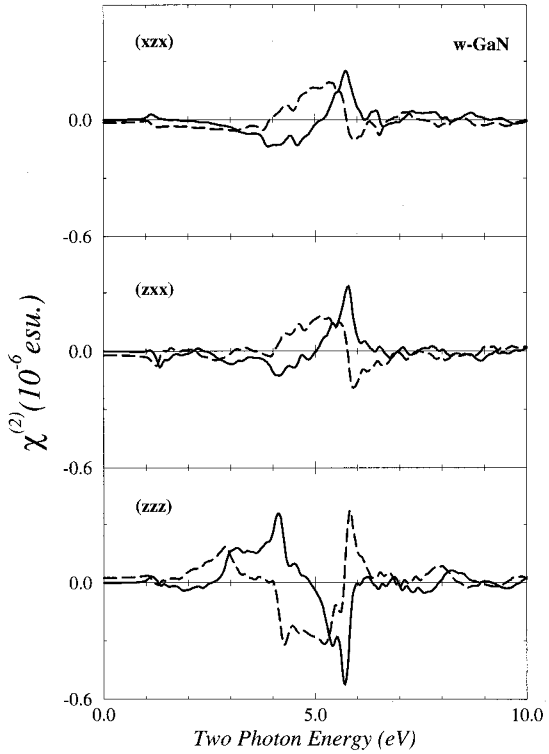

FIG. 15. The same as Fig. 11 but for a wurtzite GaN crystal.

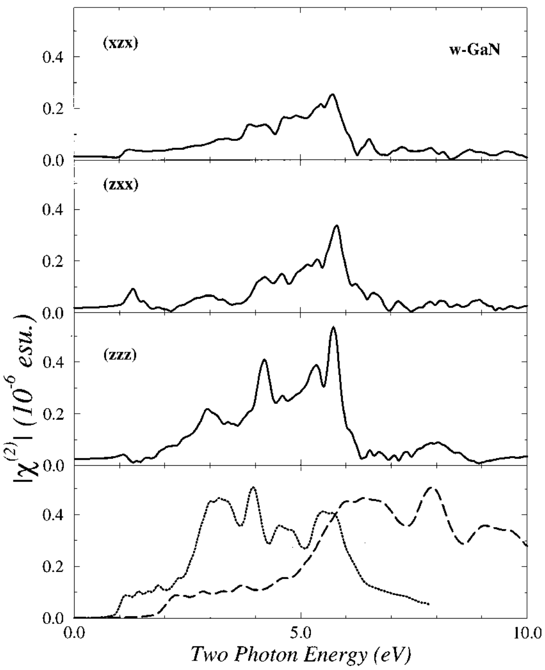

FIG. 16. The same as Fig. 12 but for a wurtzite GaN crystal.

For cubic AlN the calculated SHG spectrum agrees well with the previous LMTO-ASA result.[20] However, there are some differences in their line shapes. Our FLAPW theory predicts a stronger response in the spectral region above 6 eV. As mentioned above, our FLAPW calculations for InN predict a stronger linear response in the low-energy spectral region than the previous LMTO-ASA study,[2] (cf. Fig. 5), due

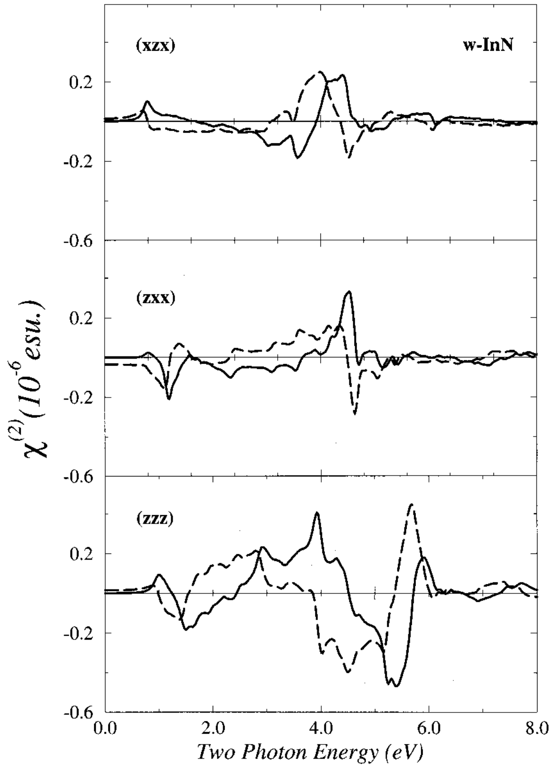

FIG. 17. The same as Fig. 11 but for a wurtzite InN crystal.

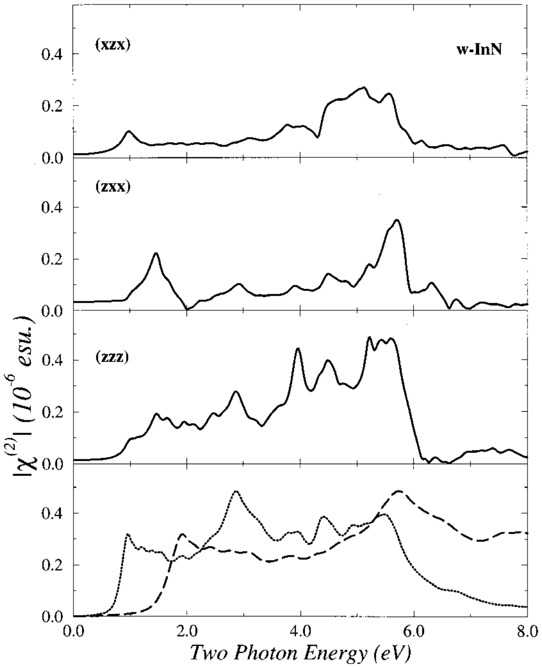

FIG. 18. The same as Fig. 12 but for a wurtzite InN crystal.

mainly to a better description of wave functions, charge, and potential in the FLAPW method.

D. Role of the *d* states

As shown in Figs. 1 and 2, the *d* states of GaN and InN are located at about 14 eV below the Fermi level. Weak hybridization exists between *d* states of adjacent atoms. To understand the role of the *d* states in the linear and nonlinear optical response functions we calculated $\epsilon(\omega)$ and $\chi^{(2)}$ of GaN and InN without inclusion of optical transitions from/to the *d* states. We found that optical transitions related to the *d* states provide remarkable contributions in both materials. As an example, the results obtained for GaN are shown by thin lines in Fig. 19 in comparison with the data of the precise calculations. The imaginary part of dielectric functions in the upper panel of Fig. 19 is obviously reduced by excluding *d*-state transitions at $\hbar\omega > 6.0$ eV. Consequently, the value of the static dielectric constant decreases by about 15%. The nonlinear susceptibility is affected even more strongly [see Fig. 19(b)], because the two-photon processes involve much more electronic states around the Fermi level than in the linear response. Our results demonstrate that electron transitions involving *d* states contribute in the whole spectral range of $\chi^{(2)}$, and the related corrections are possibly as large as 50%.

E. Optical response: Wurtzite versus cubic structure

The group-III nitrides often exist in mixed structures with cubic and hexagonal phases. It is thus important to understand how sensitive the SHG is to the changes in the crystalline structure. In both cubic (zinc-blende) and wurtzite structures each atom of one kind is tetrahedrally surrounded by four atoms of the other kind. Because both phases have the same nearest-neighbor configurations, one may expect similar optical responses.

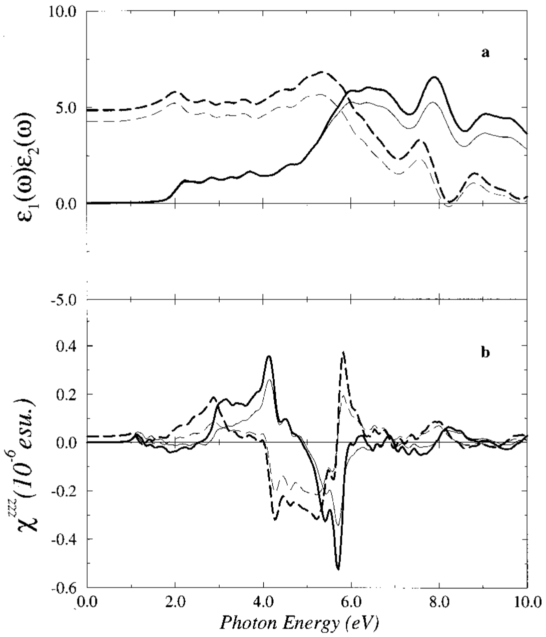

FIG. 19. The calculated spectra of (a) real (dashed lines) and imaginary parts (solid lines) of linear dielectric functions $\epsilon=\epsilon_1+i\epsilon_2$, and (b) real (dashed lines) and imaginary parts (solid lines) of $\chi^{(2)}_{zzz}$ of the wurtzite GaN crystal. The thin lines are corresponding values calculated by excluding *d* states from the optical transition matrix elements.

The first systematic study of linear and second-order optical susceptibilities in cubic and hexagonal II-VI semiconductors[44] indicated that the change in atomic structure plays a limited role at energies below the gap (linear functions) or at half gap (second-order response). Stronger effects were reported in the high-energy regions of II-VI compounds.[44]

In this work we compare the imaginary parts of the $\chi^{(2)}_{zzz}$ component for group-III nitrides with $\chi^{(2)}_{xyz}$ spectra for both wurtzite and cubic structures in Fig. 20. Following Ref. 44, we project the $\chi^{(2)}_{xyz}$ component of the cubic structure into the hexagonal frames. As in II-VI semiconductors,[44] the spectra of two nitride phases are very different. For GaN and InN the $\chi^{(2)}$ spectra for the two structures are similar only in the long-wavelength regions. The spectra of the cubic phase are remarkably blueshifted in the high-energy region. These differences around direct-gap energies can be explained. The localization of optical transitions in **k** space corresponds to a delocalization in the real space. In other words, electron transitions around direct optical gaps may involve atomic bonds extending to several atomic shells in the real space.

Comparing SHG results of the two phases (see Fig. 20) one can see that $\chi^{(2)}$ spectra in cubic materials are systematically blueshifted with respect to their hexagonal counterparts. This corresponds to the structure-induced changes in the bandwidth and gap sizes. Although the LDOS for the two phases in Figs. 1 and 2 is very close in profile, the bands of wurtzite crystals are noticeably narrower. It is well known that the electron band structure of solids is determined mainly through the interactions between nearest neighbors, with much weaker contributions from the interactions with the second-nearest neighbors, and the interactions with third-nearest neighbors very offen could be neglected for the

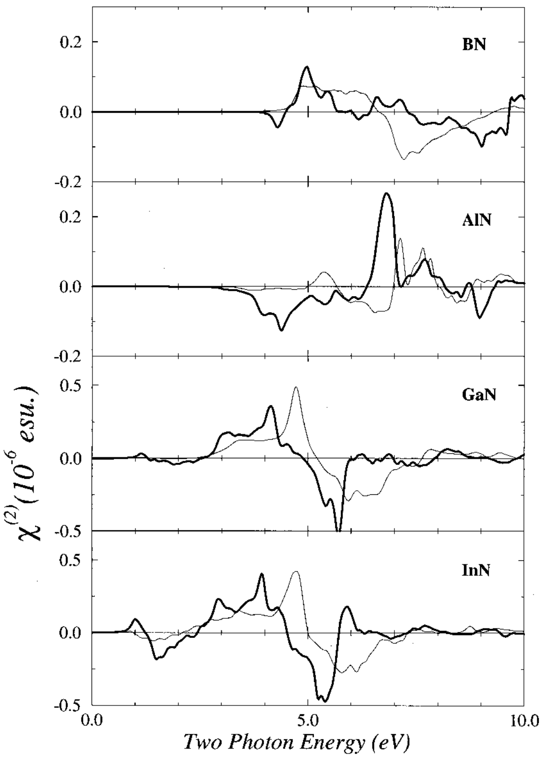

FIG. 20. The calculated spectra of the imaginary second-order optical susceptibility components of the wurtzite ($\chi^{(2)}_{zzz}$, bold lines) and of the zinc-blende ($\chi^{(2)}_{xyz}$, thin lines) crystals. The optical functions of the cubic phase are projected into the hexagonal coordinate frames.

estimations.[45] Atomic geometries of the two phases are the same up to second-nearest neighbors. As a consequence of the same atomic configuration in the first two atomic shells in cubic and wurztite crystals, the shapes of the SHG spectra of two phases are quite similar (see Fig. 20). Note from the lattice parameters in Tables I and V, the nearest- and second-nearest-neighbor interatomic distances in the wurtzite structure are 0.1–0.6 % larger than those in the cubic phase (in agreement with corresponding data calculated for ideal structures using experimental lattice constants). The increase of d_{12} and d_{13} causes the weakening of the relevant bonding energies and gives rise to the obtained redshift of the SHG spectra in hexagonal as compared to the zinc-blende crystals.

TABLE V. Calculated distances (in Å) between nearest (d_{12}) and second-nearest neighbors (d_{13}) of zinc-blende and wurtzite (in parentheses) nitrides.

	BN	AlN	GaN	InN
d_{12}	1.567 (1.569)	1.914 (1.916)	1.970 (1.982)	2.174 (2.196)
d_{13}	2.559 (2.576)	3.120 (3.122)	3.217 (3.219)	3.550 (3.568)

By contrast the linear optical functions appear to be very stable in the cubic-hexagonal phase transitions. Clearly, the nonlinear optical response is much more sensitive to the atomic configurations than the linear one. The high sensitivity of $\chi^{(2)}$ to the atomic structure can be used for optical detections of phase mixture, embedding, and phase transitions in nitrides.

V. CONCLUSIONS

The electronic band structures and linear and nonlinear optical functions of the cubic and hexagonal BN, AlN, GaN, and InN crystals have been studied with the first-principles FLAPW method. In BN and AlN the valence bands are dominated by $2s$ and $2p$ bonding states of N. The calculated band-structure parameters and the values of macroscopic dielectric constants as well as the static values of the second-order susceptibility agree well with available data in the literature. The predicted second-order optical spectra show pronounced structures related to single- and double-frequency resonances. The SHG response in group-III nitrides is mainly due to double-frequency resonances; single-photon resonances provide noticeable contribution only in materials with heavy metals. In these materials the transitions from/to d states contribute remarkably to the linear and nonlinear optical functions. The second-order optical susceptibility functions are very sensitive to the atomic configurations in wurtzite and zinc-blende phases.

ACKNOWLEDGMENTS

Work was supported by the Division of Chemical Science, office of Basic Energy Science, U.S. Department of Energy (Grant No. DE-FG03-99ER14948) and by a computing grant at NERSC.

---

*Author to whom correspondence should be addressed. Electronic address: vgavrile@newton.csun.edu

[1] *Properties of Group III Nitrides*, edited by J. H. Edgar (EMIS, London, 1994).

[2] N. E. Christensen and I. Gorczyca, Phys. Rev. B **50**, 4397 (1994).

[3] S. Logothetidis, J. Petalas, M. Cardona, and T. D. Moustakas, Phys. Rev. B **50**, 18 017 (1994).

[4] W. R. L. Lambrecht, B. Segall, S. Strite, G. Martin, A. Agarwal, H. Morkọc, and A. Rockett, Phys. Rev. B **50**, 14 155 (1994).

[5] A. F. Wright and J. S. Nelson, Phys. Rev. B **50**, 2159 (1994); **51**, 7866 (1995).

[6] W. G. Aulbur, L. Jönsson, and J. W. Wilkins, Phys. Rev. B **54**, 8540 (1996).

[7] W. Shan, T. J. Schmidt, X. H. Yang, J. J. Song, and B. Goldenberg, Appl. Phys. Lett. **66**, 985 (1995).

[8] F. B. J. Y. Duboz, E. Rosencher, F. Scholz, and V. Härle, Phys. Rev. B **54**, 8116 (1996).

[9] C. B. Stagarescu, L.-C. Duda, K. E. Smith, J. H. Guo, J. Nordgren, R. Singh, and T. D. Moustakas, Phys. Rev. B **54**, R17 335 (1996).

[10] D. Vogel, P. Krüger, and J. Pollmann, Phys. Rev. B **55**, 12 836 (1997).

[11] Q. Guo, M. Nishino, H. Ogawa, and A. Yoshida, Phys. Rev. B **55**, R15 987 (1997).

[12] X. Tang, Y. Yuan, K. Wongchotigul, and M. Spencer, Appl. Phys. Lett. **70**, 3206 (1997).

[13] K. Shimada, T. Sota, and K. Suzuki, J. Appl. Phys. **84**, 4951 (1998).

[14] K. Karch and F. Bechstedt, Phys. Rev. B **56**, 7404 (1997).

[15] K. Karch, J.-M. Wagner, and F. Bechstedt, Phys. Rev. B **57**, 7043 (1998).

[16] J. Chen, Z. H. Levine, and J. W. Wilkins, Appl. Phys. Lett. **66**, 1129 (1995).

[17] H. Y. Zhang, X. H. He, Y. H. Shih, M. Schurman, Z. C. Feng, and R. A. Stall, Appl. Phys. Lett. **69**, 2953 (1996).

[18] J. Chen, L. Jönsson, J. W. Wilkins, and Z. H. Levine, Phys. Rev. B **56**, 1787 (1997).

[19] J. L. P. Hughes, Y. Wang, and J. E. Sipe, Phys. Rev. B **55**, 13 630 (1997).

[20] S. N. Rashkeev, W. R. L. Lambrecht, and B. Segall, Phys. Rev. B **57**, 3905 (1998).

[21] Y. R. Shen, *The Principles of Nonlinear Optics* (Wiley, New York, 1994).

[22] V. I. Gavrilenko, R. Wu, and M. Downer, Bull. Am. Phys. Soc. **44** (1), 1910 (1999).

[23] J. I. Dadap, Z. Xu, X. F. Hu, M. C. Downer, N. M. Russel, J. G. Ekerdt, and O. A. Aktsipetrov, Phys. Rev. B **56**, 13 367 (1997).

[24] F. Bechstedt, K. Tenelsen, B. Adolph, and R. Del Sole, Phys. Rev. Lett. **78**, 1528 (1997).

[25] R. Atanasov, F. Bassani, and V. M. Agranovich, Phys. Rev. B **50**, 7809 (1994).

[26] V. I. Gavrilenko and F. Bechstedt, Phys. Rev. B **55**, 4343 (1997).

[27] E. Wimmer, H. Krakauer, M. Weinert, and A. J. Freeman, Phys. Rev. B **24**, 864 (1981), and references therein.

[28] D. D. Koelling and B. N. Harmon, J. Phys. C **10**, 3107 (1977).

[29] J. L. P. Hughes and J. E. Sipe, Phys. Rev. B **53**, 10 751 (1996).

[30] O. K. Andersen, Phys. Rev. B **12**, 3060 (1975).

[31] U. von Barth and L. Hedin, J. Phys. C **5**, 1629 (1972).

[32] J. P. Perdew, K. Burke, and Y. Wang, Phys. Rev. B **54**, 16 533 (1996).

[33] A. J. Freeman and R. Wu, J. Magn. Magn. Mater. **100**, 497 (1992).

[34] J. E. Sipe and E. Ghahramani, Phys. Rev. B **48**, 11 705 (1993).

[35] B. Adolph and F. Bechstedt, Phys. Rev. B **57**, 6519 (1998).

[36] V. I. Gavrilenko and F. Rebentrost, Appl. Phys. A: Mater. Sci. Process. **60**, 143 (1995).

[37] M. S. Hybertsen and S. G. Louie, Phys. Rev. B **34**, 5390 (1986); **35**, 5585 (1987).

[38] Z. H. Levine and D. C. Allan, Phys. Rev. B **43**, 4187 (1991).

[39] R. W. Godby, M. Schlüter, and L. J. Sham, Phys. Rev. B **37**, 10 159 (1988).

[40] M. P. Surh, S. G. Louie, and M. L. Cohen, Phys. Rev. B **43**, 9126 (1991).

[41] Y. Osaka, A. Chayahara, H. Yokoyama, M. Okamoto, T. Hamada, and M. Fujisawa, in *Synthesis and Properties of Boron Nitride*, edited by J. J. Pouch and S. A. Alteroviz (Trans. Tech., Ädermannsdorf, Switzerland, 1990), p. 227.

[42] Q. Guo, O. Kato, M. Fujisawa, and A. Yoshida, Solid State Commun. **83**, 721 (1992).

[43] J. E. Sipe, A. I. Shkrebtii, and O. Pulci, Phys. Status Solidi A **170**, 431 (1998).

[44] J. L. P. Hughes and J. E. Sipe, Phys. Rev. B **58**, 7761 (1998).

[45] W. A. Harrison, *Electronic Structure and Properties of Solids* (Freeman, San Francisco, 1980).

[46] *Numerical Data and Functional Relationships in Science and Technology*, edited by O. Madelung, M. Schulz, and H. Weiss Landolt-Börnstein, New Series, Group III, Vol. 17, pt. a (Springer, Berlin, 1982).

[47] I. Petrov, E. Mojab, R. C. Powell, and J. E. Greene, Appl. Phys. Lett. **60**, 2491 (1992).

[48] S. Strite, J. Rujan, Z. Li, A. Salvador, H. Chen, D. J. Smith, W. J. Choyke, and H. Morkoç, J. Vac. Sci. Technol. B **9**, 1924 (1991).

[49] S. Strite, D. Chandrasekhar, D. J. Smith, J. Sariel, H. Chen, N. Teraguchi, and H. Morkoç, J. Cryst. Growth **127**, 204 (1993).

[50] T. Soma, S. Sawaoka, and S. Saito, Mater. Res. Bull. **9**, 755 (1974).

[51] H. Schulz and K. H. Thiemann, Solid State Commun. **23**, 815 (1977).

[52] K. Osamura, S. Naka, and Y. Murakami, J. Appl. Phys. **46**, 3432 (1975).

[53] U. Köhler, D. J. As, B. Schöttker, T. Frey, K. Lischka, J. Scheiner, S. Shokhovets, and R. Goldhahn, J. Appl. Phys. **85**, 404 (1999).

[54] E. Franke, M. Schubert, J.-D. Hecht, H. Neumann, T. E. Tiwald, D. W. Thompson, H. Yao, J. A. Woollam, and J. Hahn, J. Appl. Phys. **84**, 526 (1998).

[55] L. Akasaki and M. Hashimoto, Solid State Commun. **5**, 851 (1967).

[56] P. Perlin, I. Gorczyca, N. E. Christensen, I. Grzegory, H. Teisseyre, and T. Suski, Phys. Rev. B **45**, 13 307 (1992).

[57] J. Misek and F. Srobar, Electrotech. Cas. **30**, 690 (1979).

[58] A. S. Barker and M. Ilegems, Phys. Rev. B **7**, 743 (1973).

[59] T. Wethkamp, K. Wilmwrs, C. Cobet, N. Esser, W. Richter, O. Ambacher, M. Stutzmann, and M. Cardona, Phys. Rev. B **59**, 1845 (1999).

[60] A. Agui, S. Shin, M. Fujisawa, Y. Tezuka, T. Ishii, Y. Muramatsu, O. Mishima, and K. Era, Phys. Rev. B **55**, 2073 (1997).